PIBB 生物化学与生物物理进展
Progress in Biochemistry and Biophysics
XXXX, XX(XX): 1~17
www.pibb.ac.cn

Network Pharmacology and Experimental Verification Unraveled The Mechanism of Pachymic Acid in The Treatment of Neuroblastoma*

LIU Hang[1,2], ZHU Yu-Xin[1], GUO Si-Lin[1], PAN Xin-Yun[1], XIE Yuan-Jie[2,3], LIAO Si-Cong[4], DAI Xin-Wen[5], SHEN Ping[2,3]**, XIAO Yu-Bo[1,4]**

([1]*Hunan Provincial Key Laboratory for Synthetic Biology of Traditional Chinese Medicine, School of Medical Laboratory Science, Hunan University of Medicine, Huaihua* 418000, China;
[2]*Guangxi Key Laboratory of Diabetic Systems Medicine, Guilin Medical University, Guilin* 541199, China;
[3]*Joint Laboratory of Translational Medicine by Shaodong People's Hospital & Hunan Mingshun Pharmaceutical Co., Ltd, Shaodong People's Hospital, Shaodong* 422800, China;
[4]*Guangxi Key Laboratory of Molecular Medicine in Liver Injury and Repair, the Affiliated Hospital of Guilin Medical University, Guilin* 541001, China;
[5]*Expert Workstation of Hunan Butian Pharmaceutical Co., Ltd., Changsha* 410000, China)

Graphical abstract

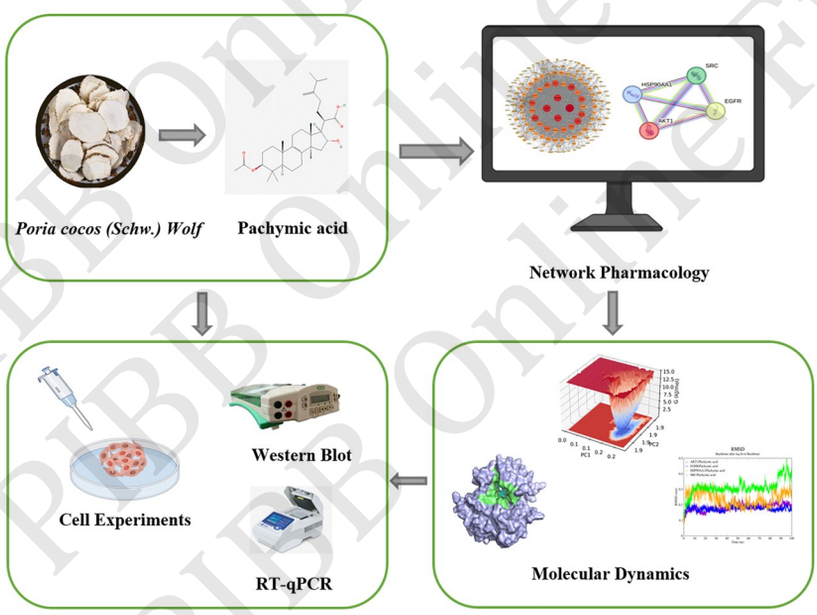

Abstract **Objective** Traditional Chinese medicine (TCM) constitutes a valuable cultural heritage and an important source of antitumor compounds. *Poria* (*Poria cocos* (Schw.) Wolf), the dried sclerotium of a polyporaceae fungus, was first documented in

* This work was supported by grants from the Hunan Provincial Natural Science Foundation (2023JJ50440), the Natural Science Foundation of Guangxi (2025GXNSFHA069221), the Scientific Research Fund of Hunan Provincial Education Department (22A0707), the National College Student Innovation and Entrepreneurship Training Program (S202212214001), the Guangxi Health Commission Key Laboratory of Basic Research in Sphingolipid Metabolism Related Diseases (GKLBRSMR-K202403), and Horizontal Cooperation Research Project of Shaodong People's Hospital (2023SDHX02).
** Corresponding author.
SHEN Ping. Tel: 86-739-2721153, E-mail: shenpsd@126.com
XIAO Yu-Bo. Tel: 86-745-2381486, E-mail: yuboxiaohn@126.com
Received: April 9, 2025 Accepted: June 13, 2025

Shennong's Classic of Materia Medica and has been used therapeutically and dietarily in China for millennia. Traditionally recognized for its diuretic, spleen-tonifying, and sedative properties, modern pharmacological studies confirm that *Poria* exhibits antioxidant, anti-inflammatory, antibacterial, and antitumor activities. Pachymic acid (PA; a triterpenoid with the chemical structure 3β-acetyloxy-16α-hydroxy-lanosta-8,24(31)-dien-21-oic acid), isolated from *Poria*, is a principal bioactive constituent. Emerging evidence indicates PA exerts antitumor effects through multiple mechanisms, though these remain incompletely characterized. Neuroblastoma (NB), a highly malignant pediatric extracranial solid tumor accounting for 15% of childhood cancer deaths, urgently requires safer therapeutics due to the limitations of current treatments. Although PA shows multi-mechanistic antitumor potential, its efficacy against NB remains uncharacterized. This study systematically investigated the potential molecular targets and mechanisms underlying the anti-NB effects of PA by integrating network pharmacology-based target prediction with experimental validation of multi-target interactions through molecular docking, dynamic simulations, and *in vitro* assays, aimed to establish a novel perspective on PA's antitumor activity and explore its potential clinical implications for NB treatment by integrating computational predictions with biological assays. **Methods** This study employed network pharmacology to identify potential targets of PA in NB, followed by validation using molecular docking, molecular dynamics simulations, MM/PBSA free energy analysis, RT-qPCR and Western blot experiments. Network pharmacology analysis included target screening *via* TCMSP, GeneCards, DisGeNET, SwissTargetPrediction, SuperPred, and PharmMapper, Subsequently, potential targets were predicted by intersecting the results from these databases *via* Venn analysis. Following target prediction, topological analysis was performed to identify key targets using Cytoscape software. Molecular docking was conducted using AutoDock Vina, with the binding pocket defined based on crystal structures. Molecular dynamics (MD) simulations were performed for 100 ns using GROMACS, and RMSD, RMSF, SASA, and hydrogen bonding dynamics were analyzed. MM/PBSA calculations were carried out to estimate the binding free energy of each protein-ligand complex. *In vitro* validation included RT-qPCR and Western blot, with GAPDH used as an internal control. **Results** The CCK-8 assay demonstrated a concentration-dependent inhibitory effect of PA on NB cell viability. GO analysis suggested that the anti-NB activity of PA might involve cellular response to chemical stress, vesicle lumen, and protein tyrosine kinase activity. KEGG pathway enrichment analysis suggested that the anti-NB activity of PA might involve the PI3K/Akt, MAPK, and Ras signaling pathways. Molecular docking and MD simulations revealed stable binding interactions between PA and the core target proteins AKT1, EGFR, SRC, and HSP90AA1. RT-qPCR and Western blot analyses further confirmed that PA treatment significantly decreased the mRNA and protein expression of AKT1, EGFR, and SRC while increasing the HSP90AA1 mRNA and protein levels. **Conclusion** It was suggested that PA may exert its anti-NB effects by inhibiting AKT1, EGFR, and SRC expression, potentially modulating the PI3K/Akt signaling pathway. These findings provide crucial evidence supporting PA's development as a therapeutic candidate for NB.

Key words pachymic acid, network pharmacology, molecular dynamics simulation

DOI：10.16476/j.pibb.2025.0154 **CSTR**：32369.14.pibb.20250154

Neuroblastoma (NB), a malignant neoplasm originating from the sympathetic nervous system, predominantly occurs in the cervical region, mediastinum, adrenal glands, peritoneum, or presacral areas. As the second most prevalent extracranial malignancy in pediatric populations, it constitutes the most common solid tumor in infants, with approximately 75% of cases manifesting in children under 5 years of age, half of which are classified as high-risk[1-2]. Current clinical management relies primarily on surgical resection. However, the anatomical proximity of NB lesions to major vascular structures (*e.g*., the aorta and vena cava) often leads to tumor extension into the spinal canal *via* intervertebral foramina, resulting in spinal cord compression and increased surgical complexity. Consequently, the 5-year survival rate remains below 30%[2-3], underscoring the urgent need for developing novel pharmacological interventions with improved safety and efficacy.

Traditional Chinese medicine (TCM), which is a valuable cultural heritage, has emerged as an important source of compounds for antitumor drug discovery. *Poria* (*Poria cocos* (Schw.) Wolf), the dried sclerotium of the polyporaceae fungus, was first documented in *Shennong's Classic of Materia Medica* and has been used for millennia in China for both therapeutic and dietary purposes. *Poria* is traditionally recognized for its diuretic, spleen-tonifying, and sedative properties, and modern pharmacological studies have demonstrated that it has exhibits antioxidant, anti-inflammatory, antibacterial, and

antitumor activities[4]. Pachymic acid (PA; 3β-acetyloxy-16α-hydroxy-lanosta-8, 24(31)-dien-21-oic acid), a triterpenoid compound isolated from *Poria*, is considered one of its principal bioactive constituents.

Emerging evidence has demonstrated that PA has antitumor potential through multiple mechanisms: (1) induction of cell cycle arrest and apoptosis in gastric cancer cells[5]; (2) suppression of gallbladder cancer *via* modulation of the AKT and ERK signaling pathways[6]; (3) activation of Caspase 3/7 and regulation of the PTEN/AKT pathway in osteosarcoma cells[7]; and (4) inhibition of hypoxia/HIF-1α-mediated Bax expression in gastric cancer[8]. These collective findings suggest that PA has broad-spectrum antitumor activity. While our preliminary experiments revealed concentration-dependent anti-NB effects on cell viability, the underlying mechanisms remain uncharacterized, necessitating further investigation.

With the gradual rise of interdisciplinary subjects such as computational biology, bioinformatics, artificial intelligence, and big data science, researchers have shifted studies of traditional medicine from a single and isolated mode to a multi-faceted and systematic mode. One of the significant changes is understanding the mechanisms of drug action from the perspective of the biomolecular network[9-10]. Network pharmacology stems from several pioneering works. The holistic theory and practice of TCM play key roles in the origin and rapid development of network pharmacology. The original hypothesis referring to the biological associations between TCM syndromes, herbal formulas, and molecular networks was proposed in 1999 and 2002[9]. A milestone article proposed a new network-based TCM research paradigm in 2007[11]. The new term "network pharmacology" was introduced in *Nature Biotechnology* by Hopkins[12].

This approach integrates bioinformatics and computational biology to predict drug targets and pharmacodynamic processes, significantly accelerating drug development. Recent advancements in bioinformatics resources have expanded its applications in drug screening and mechanistic studies. For example, Liu *et al*. [13] successfully employed network pharmacology to identify the therapeutic potential of Astragalus flavonoids in diabetic nephropathy, which was subsequently validated through *in vitro* experiments. However, experimental validation remains crucial for ensuring the reliability of the results. In combination with network pharmacology, molecular docking predicts ligand-receptor interactions through spatial configuration and electrostatic analyses[14]. This technique enables presynthesis evaluation of bioactive compounds, reducing experimental costs and timelines. Xu *et al*. [15] demonstrated its utility by identifying the *cis*-isomer of the PI3K inhibitor 6g as having superior antitumor activity compared to its trans-isomer, a finding later confirmed by in vitro testing. Furthermore, molecular dynamics (MD) simulations address the static limitations of docking by modeling dynamic protein-ligand interactions under physiological conditions, allowing quantitative assessment of binding free energy and complex stability.

In this study, we integrate network pharmacology, molecular docking, and MD simulations to systematically investigate the anti-NB mechanisms of PA. This multimodal approach aims to identify potential therapeutic targets and establish a theoretical foundation for the development of novel NB treatments.

1 Methods

1.1 Databases and software

This study utilized the following databases for data collection and analysis: SwissTargetPrediction (http://swisstargetprediction. ch/), Genecards (https://www.genecards.org), OMIM (https://omim.org), TTD (https://db. idrblab. net/ttd/), PharmGkb (https://www.pharmgkb.org/), Drugbank (http://www.drugbank.ca/), SuperPRED (https://prediction. charite. de/), PubChem (https://pubchem. ncbi. nlm. nih. gov), DAVID (https://david. ncifcrf. gov), and PDB (https://www. rcsb. org/). Software tools included Cytoscape 3.7.2, Pymol 2.5, and AutoDock 1.5.7.

1.2 Drug target prediction

PA's chemical formula was input into the SwissTargetPrediction, SuperPred, and PharmMapper databases for target prediction. SwissTargetPrediction predicts drug targets based on known chemical structures of drug molecules, covering targets across human, mouse, and rat species, with over 300 000 known compounds and 3 000 targets. SuperPred predicts drug targets by extracting drug-target interaction data from BindingDB, SuperTarget, and

ChEMBL, encompassing approximately 340 000 compounds and thousands of targets. PharmMapper uses pharmacophore models to predict target proteins, containing over 50 000 unique pharmacophore models. The database was used in September 2024.

1.3 Neuroblastoma target retrieval

Using the keyword "neuroblastoma" relevant therapeutic targets were identified from TTD, PharmGKB, OMIM, Genecards, and Drugbank databases. TTD contains over 5 000 drug targets and hundreds of targets for approved drugs. PharmGKB, a leading pharmacogenomics resource supported by the National Institutes of Health (NIH), provides comprehensive pharmacogenomics data. OMIM is an evolving human genetic information database with over 16 000 gene entries. GeneCards is a comprehensive database integrating transcriptomics, genomics, and proteomics information, while Drugbank is a reliable bioinformatics database of experimentally validated drug data. The retrieval time of the database was all in September 2024.

1.4 GO and KEGG enrichment analyses

Genes meeting the *P.*adjust<0.001 criterion were used for enrichment analysis. Gene ontology (GO) functional enrichment analysis was performed using the DAVID database (https://davidbioinformatics.nih.gov/) [16], while pathway enrichment analysis was conducted using the Kyoto Encyclopedia of Genes and Genomes (KEGG) pathway database[17]. GO functional annotation graphics were generated *via* the Bioinformatics website (https://www.bioinformatics.com.cn/). The database was used in September 2024. Firstly, GO terms that were preliminarily considered to be significantly enriched in the gene set enrichment analysis were screened out with a *P*-value<0.05. Then, the original *P*-values were corrected using the Bonferroni correction method to obtain the *P.*adjust values or *q*-values. These corrected *P*-values were used to control the proportion of false positive discoveries.

1.5 PPI network construction

Using the STRING database (https://cn.string-db.org/) for protein-protein interaction (PPI) network analysis, important nodes within the target proteins were identified by constructing the PPI network[18]. The database was used in September 2024.

1.6 Molecular docking for PA target validation

Molecular docking was performed to validate network pharmacology results by predicting the binding interactions between PA and relevant target proteins. Structures of small-molecule ligands and target protein receptors were obtained from the PubChem and PDB databases. Preprocessing and identification of active pockets were done using Pymol and AutoDock software, with binding modes assessed based on binding energy. The database was used in September 2024.

1.7 Molecular docking

Molecular docking was used to study the molecular affinity of the small molecule PA to core target protein. The protein crystal structures were downloaded from the PDB database, and 3D structures of small molecules were downloaded from the PUBCHEM database. We performed the molecular docking work by employing AutoDock Vina 1.1.2 software[19]. Prior to docking, PyMol 2.5 was used to process all receptor proteins (including removal of water molecules, salt ions and small molecules). ADFRsuite 1.0 was used to convert all processed small molecules and receptor proteins into the PDBQT format required for docking with AutoDock Vina 1.1.2[20]. The docked conformation with the highest molecular docking score was considered to be the binding conformation for subsequent molecular dynamics simulations. We analyzed and compared the binding site poses, chemical bond lengths and chemical bond angles of the original crystal ligand to the protein by re-docking the original crystal ligand and the protein using the original crystal ligand of the protein target as a positive reference. Finally, the consistency of the binding mode can indicate the correctness of the molecular docking scheme.

1.8 Molecular dynamics simulations

Based on the docking results, the best-posed complex was subjected to MD simulation studies using the Groningen Machine for Chemicals Simulations (GROMACS) 5.0 package with a CHARMM36 force field[21] under periodic boundary conditions for molecules. Ligand topology files were generated using the CHARMM General Force Field[22]. The charge of the system was neutralized by the addition of the ions. The energy was minimized using a steepest-gradient method to remove any close contacts. The particle mesh Ewald (PME) method was employed for energy calculation and for electrostatic

and van der Waals interactions. The systems were equilibrated in the NVT ensemble for 50 000 steps, followed by equilibration in the NPT ensemble for an additional 50 000 steps. Finally, 100 ns molecular dynamics simulations were performed at 26.85℃ with a 2.0 fs time step, and coordinates were saved every picosecond for analysis[23-24].

1.9 Molecular Mechanics/Poisson Boltzmann（Generalized Born） Surface Area binding free energy calculation

The Molecular Mechanics/Poisson Boltzmann (GeneralizedBorn) Surface Area (MM-PBSA) method was used to calculatethe free energy of binding between proteins and ligands[25]. We used 100 ns molecular dynamics simulations forthe calculation. The calculation equation is as follows:

$$\Delta G_{bind} = \Delta G_{complex} - \left(\Delta G_{receptor} + \Delta G_{ligand}\right) = \Delta E_{internal} + \Delta E_{vdw} + \Delta E_{elec} + \Delta G_{PB} + \Delta G_{SA}$$

ΔG_{bind} is the binding free energy, which serves as a key parameter for evaluating the stability and affinity of the interaction between the ligand and the target protein. A more negative value indicates a more favorable binding interaction. $\Delta G_{complex}$, $\Delta G_{receptor}$, ΔG_{ligand} are the total free energies of the ligand-receptor complex, the unbound receptor, and the unbound ligand, respectively. The difference between these terms is used to estimate the energy change during the binding process. $\Delta E_{internal}$ is the internal energy of the molecule, including bond, angle, and dihedral energies. This term reflects the extent of conformational changes induced by binding. ΔE_{vdw} (van der Waals energy) represents van der Waals interactions, describing non-specific interactions between molecules, particularly those associated with hydrophobic contacts. ΔE_{elec} (electrostatic energy) refers to the electrostatic (coulombic) interactions between charged atoms within the system, which are critical for determining the specificity and strength of the binding. ΔG_{PB} is the polar solvation free energy, calculated using the Poisson–Boltzmann (PB) model. It accounts for the electrostatic interactions between the solute's charged groups and the surrounding polar solvent, such as water. ΔG_{SA} is the nonpolar solvation free energy, usually estimated based on the solvent-accessible surface area (SASA). This term reflects the contribution of hydrophobic effects to the overall binding process.

1.10 CCK−8 assay for assessing cell viability

Neuro-2a (N2a) neuroblastoma cells were seeded at a density of 1×10^4 cells per well in 96-well plates. After exposure to varying concentrations of PA for a duration of 24 h, 100 μl of the Cell Counting Kit-8 (CCK-8) reagent was added to each well. The plates were then incubated at 37° C for 2 h. Absorbance readings were obtained at a wavelength of 450 nm using a microplate reader. Cell viability was subsequently determined using the formula: (absorbance of experimental group)/(absorbance of control group)×100%.

1.11 RT–qPCR for core gene expression analysis

Total RNA was isolated from cells using Trizol reagent and quantified with a Nanodrop 2000 spectrophotometer. Reverse transcription was conducted using a reverse transcription kit, and quantitative PCR (RT-PCR) was performed with SYBR-Green reagent. The reaction conditions were as follows: the qPCR procedure consisted of an initial uracil-DNA glycosylase (UDG) reaction at 37°C for 2 min, followed by pre-denaturation at 95°C for 3 min. The amplification was carried out for 40 cycles, with each cycle comprising denaturation at 95° C for 5 s and annealing/extension at 60° C for 30 s. Relative gene expression was calculated using the $2^{-\Delta\Delta Ct}$ method, with $P<0.05$ considered statistically significant. Primer sequences are listed in Table 1.

Table 1　Primer sequences for RT–qPCR

Gene	Forward	Reverse
AKT1	5’-CCTCTGCTTTGTCATGGAGTACG-3’	5’-AGCCCGAAGTCTGTGATCTTAAT-3’
EGFR	5’-ACAGCATAGACGACACCTTCCTC-3’	5’-TGGCTTGGACACTGGAGACTG-3’
SRC	5’-TGGTTTCAGAGGAGCCCATTTAC-3’	5’-CACTTTGCACACCAGGTTCTCTC-3’
HSP90AA1	5’-CACGTCTCTGCATTCCCTGTCAC-3’	5’-GTCTCAACCTCCTCCTCCTCCATC-3’
β-actin	5’-GTGCTATGTTGCTCTAGACTTCG-3’	5’-ATGCCACAGGATTCCATACC-3’

1.12 Western blot

Total protein was extracted from cells using RIPA lysis buffer supplemented with protease and phosphatase inhibitors and quantified *via* BCA assay. Proteins (30 μg per sample) were separated by 12% SDS-PAGE and transferred to PVDF membranes using a wet transfer system at 200 mA for 2 h. Membranes were blocked with 5% non-fat milk in TBST for 1 h at room temperature, followed by incubation with primary antibodies (diluted 1:1 000 in blocking buffer) overnight at 4° C. After 3 washes with TBST, membranes were incubated with HRP-conjugated secondary antibodies (1:5 000 dilution) for 1 h at room temperature. Protein bands were visualized using an ECL chemiluminescence detection system, and band intensities were quantified using ImageJ software. β -actin was used as a loading control, and relative protein expression levels were normalized to β -actin. Statistical significance was defined as $P<0.05$.

1.13 Statistical analysis

Data were statistically analyzed using GraphPad Prism 8. 3. 0 software. All data are represented by mean±SD. Analysis of multiple groups was performed by one-way analysis of variance (one-way ANOVA) followed by the Tukey's post hoc tests. If only 2 groups were being compared, the Student's *t* test was used. $P<0.05$ was considered statistically significant.

2 Results

2.1 Effect of PA on NB cell viability *via* the CCK−8 assay

To evaluate the effect of PA on the viability of NB cells, CCK-8 assay was performed with the N2a cell line as a model system. This assay was conducted to quantify cell viability following a 24-hour exposure to PA. As shown in Figure 1a, PA reduced the viability of N2a cells in a concentration-dependent manner, with a statistically significant decrease observed at concentrations of 10 μmol/L and 20 μmol/L after the 24-hour treatment period.

2.2 Screening and prediction of PA and NB targets

A comprehensive analysis identified 1 557 genes associated with NB from databases such as TTD, PharmGKB, OMIM, GeneCards, and DrugBank. Subsequently, predictive tools including SwissTargetPrediction, PharmMapper, and SuperPRED were utilized to forecast 471 potential PA targets. Through Venn analysis, the intersection of these datasets revealed 142 common genes, which were identified as potential PA targets for NB (Figure 1b, Table 2).

2.3 GO enrichment analysis

GO enrichment analysis was conducted on 142 PA-NB target genes, employing a selection criterion of *P.*adjust < 0.01 across the biological process (BP), cellular component (CC), and molecular function

Table 2 142 common genes identified as potential PA targets for NB

142 possible target genes for NB									
MMP2	*ERBB4*	*IGF1*	*TGFB2*	*RAC1*	*NOS2*	*SOD2*	*FGFR1*	*MET*	*ALOX5*
PTPN11	*PLK1*	*PLA2G2A*	*MAOA*	*GRB2*	*MAPK12*	*CDK1*	*PREP*	*CHEK1*	*BCHE*
ARF4	*THRB*	*KCNH2*	*ESRRA*	*TACR1*	*CAPN1*	*CASP8*	*MAPK10*	*SCN4A*	*OPRK1*
FGF1	*CHRM1*	*PPARG*	*CACNA1B*	*HSPA8*	*RARB*	*PRKCD*	*GSTP1*	*AURKA*	*ABCB1*
NFE2L2	*AURKB*	*MTOR*	*KDM1A*	*MAPK14*	*CDK6*	*CTSB*	*LCK*	*FGFR2*	*KIT*
FNTB	*EDNRB*	*FHIT*	*JAK2*	*NR1H2*	*STAT3*	*CASP1*	*SPHK1*	*XIAP*	*APAF1*
PTGS2	*ARG1*	*ADAM10*	*TGFBR1*	*CDC42*	*BMP2*	*ESR1*	*CASP7*	*HRAS*	*CTSD*
MME	*NTRK3*	*CCNA2*	*GSK3B*	*STAT1*	*ANXA5*	*RAN*	*HSP90AA1*	*CASP3*	*PARP1*
GSR	*KDR*	*HMOX1*	*RARA*	*CRABP2*	*FAP*	*TTR*	*MAOB*	*BACE1*	*NME2*
GSTM1	*MAPK1*	*PLAT*	*PIK3CG*	*MDM2*	*AKT2*	*NQO1*	*NR4A1*	*IL2*	*LGALS3*
GRIN1	*TOP2A*	*MAPK8*	*BCL2L1*	*HPRT1*	*ABL1*	*AKR1B1*	*TERT*	*HIF1A*	*METAP2*
SRC	*CDK2*	*PDE4B*	*CHRM2*	*OPRM1*	*TLR4*	*RARG*	*INSR*	*CDKN1A*	*CDK5*
ADAM17	*AKT1*	*PIK3R1*	*PDGFRA*	*IDH1*	*HDAC10*	*MIF*	*MAP2K1*	*NFKB1*	*ABCC1*
CHRM3	*DDX39B*	*ALB*	*PTGS1*	*EPAS1*	*YARS1*	*P2RX7*	*ESR2*	*BRAF*	*CYP3A4*
MMP9	*EGFR*								

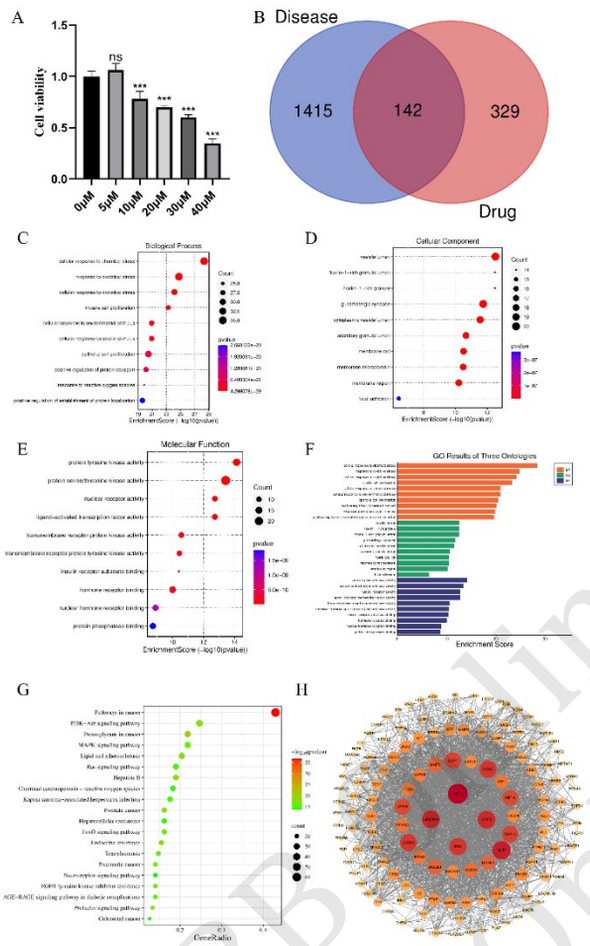

Fig. 1　Network pharmacology−based exploration of PA targets and pathways in NB

（a） CCK-8 assay results showing the viability of N2a cells treated with different concentrations of PA. （b） Venn diagram illustrating the overlapping potential targets of PA for the treatment of NB. （c－f） Gene ontology （GO） analysis of the potential targets, including biological process （BP）, molecular function （MF）, and cellular component （CC） categories. （g） KEGG pathway enrichment analysis of the potential targets, highlighting the most significantly enriched pathways. （h） Protein-protein interaction （PPI） network of the identified targets.

(MF) categories. This analysis revealed 312 biological processes, 65 cellular components, and 75 molecular functions. All significant GO enrichment results passed false discovery rate (*FDR*)<0.05 significance threshold. The top 10 results for each category were visualized, with bubble size denoting the number of differential proteins and color representing the adjusted *P*-value. A more intense red color indicates a lower P-value, signifying a stronger association. GO enrichment analysis was conducted on 142 PA-NB target genes, employing a selection criterion of *P.* adjust < 0.001 across the BP, CC, and MF categories. This analysis revealed 312 biological processes, 65 cellular components, and 75 molecular functions. The top 10 results for each category were visualized, with bubble size denoting the number of differential proteins and color representing the adjusted P value. A more intense red color indicates a lower P value, signifying a stronger association (Figure 1c－f).

2.4　KEGG enrichment analysis

KEGG pathway analysis was performed on the 142 PA-NB target genes, applying a significance threshold of *P.* adjust<0.01. All significant GO enrichment results passed FDR<0.05 significance threshold. The results were visualized according to target count and *P*-value, as illustrated in Figure 1h. Notably, pathways such as phosphoinositide 3-kinase-protein kinase B (PI3K-Akt), mitogen-activated protein kinase (MAPK), and Ras signaling pathways potentially significantly affected the anti-NB activity of PA (Figure 1g). Current research indicates that signaling pathways such as PI3K-Akt and MAPK are closely associated with the occurrence and progression of NB, suggesting that PA may exert its anti-NB effects through these pathways[26].

2.5　PPI network construction and core gene screening

The intersecting 142 PA-NB targets were subsequently imported into the STRING database to construct a PPI network, which was visualized using Cytoscape (Figure 1g). Core proteins with a degree value exceeding 60 were identified, leading to the selection of 14 high-interaction proteins, as detailed in Table 3 and Figure 1h.

2.6　Molecular docking validation of PA and key target proteins

Proteins with a degree greater than 80, including RAC-alpha serine/threonine-protein kinase (AKT1), epithelial growth factor receptor (EGFR), proto-oncogene tyrosine-protein kinase Src (SRC), and heat shock protein 90 alpha family class A member 1 (HSP90AA1), were identified as core targets. The binding affinity between a ligand and a receptor is inversely related to the binding energy; thus, a more negative binding energy denotes stronger binding. Typically, a binding energy below －4.25 kcal/mol signifies a certain degree of binding activity, whereas

Table 3 Topological parameters related to the core targets of PA and NB

Name	Protein name	Betweenness	Degree	Closeness	Clustering coefficient
AKT1	RAC-alpha serine/threonine-protein kinase	1 594.13	97	0.74	0.32
SRC	Proto-oncogene tyrosine-protein kinase Src	1 298.61	87	0.71	0.42
EGFR	Epithelial growth factor receptor	894.88	83	0.69	0.38
HSP90AA1	Heat shock protein 90 alpha family class A member 1	1 320.53	83	0.69	0.40
ALB	Albumin	1 007.89	79	0.69	0.35
HRAS	HRas proto-oncogene， GTPase	856.37	79	0.68	0.43
CASP3	Caspase 3	646.77	78	0.67	0.67
STAT3	Signal transducer and activator of transcription 3	390.06	75	0.66	0.66
ESR1	Estrogen receptor 1	597.39	74	0.66	0.66
MTOR	Mechanistic target of rapamycin kinase	261.52	72	0.65	0.65
HIF1A	Hypoxia inducible factor 1 subunit alpha	380.68	72	0.65	0.65
BCL2L1	BCL2 like 1	226.94	64	0.62	0.62
MAPK1	Mitogen-activated protein kinase 1	451.27	63	0.63	0.63
MMP9	Matrix metallopeptidase 9	495.30	63	0.62	0.62

values below －5.00 kcal/mol indicate good binding activity, and those below －7.00 kcal/mol reflect strong binding activity. As demonstrated in Table 4 and Figure 2, PA exhibited strong binding affinity with AKT1, EGFR, SRC and HSP90AA1. These findings imply that all four core proteins could contribute to the therapeutic effects of PA against NB. These results suggest that PA effectively binds to these four protein targets.

2.7 Molecular dynamics simulation of PA−target protein complexes

To further validate the stability and dynamic behavior of PA binding to core target proteins, molecular dynamics (MD) simulations were performed for the PA-AKT1, PA-EGFR, PA-SRC, and PA-HSP90AA1 complexes over 100 ns.

2.7.1 RMSD and RMSF analysis

To assess the structural stability of the protein-ligand complexes during molecular dynamics simulations, the root mean square deviation (*RMSD*) values of both the protein backbone and the ligand relative to their initial conformations were calculated (Figure 3a, b). All the complexes reached equilibrium within 10 － 20 ns, followed by relatively minor fluctuations, indicating stable and reliable simulations. Notably, the PA-HSP90AA1 and PA-SRC complexes presented lower *RMSD* values for both the backbone and ligand, suggesting stable binding conformations. In contrast, the PA-EGFR complex showed slightly greater *RMSD* fluctuations, indicating potential conformational flexibility (Figure 3b). To further investigate local flexibility and dynamic behavior, the *RMSF* of individual residues was computed for each complex (Figure 3c－f). In the PA-AKT1 complex (Figure 3c), most residues presented root mean square fluctuation (*RMSF*) values below 0.2 nm, with only minor fluctuations at the N- and C-terminal regions. This indicates a stable core domain and minimal structural perturbation upon ligand binding. In the PA-EGFR complex (Figure 3d), moderate fluctuations were observed at several residue positions, especially in loop regions and the C-terminal domain, suggesting localized conformational adaptability upon ligand interaction. The PA-HSP90AA1 complex (Figure 3e) presented the highest *RMSF* values, exceeding 1.2 nm at the N-terminal region, indicating substantial flexibility, which may be functionally relevant to its chaperone activity. In contrast, the PA-SRC complex (Figure 3f) showed consistently low fluctuations across most residues, indicating a stable conformation with only slight flexibility at terminal regions. Taken together, the RMSD and RMSF analyses revealed that the PA-SRC and PA-AKT1 complexes exhibit both global and local structural stability, whereas the PA-EGFR and PA-HSP90AA1 complexes demonstrate greater flexibility, which may play a role in their interaction mechanisms with PA.

2.7.2 Radius of gyration （Rg） and solvent accessible surface area （SASA）

The Rg values (Figure 4e) indicated that all 4 protein-ligand complexes maintained relatively stable

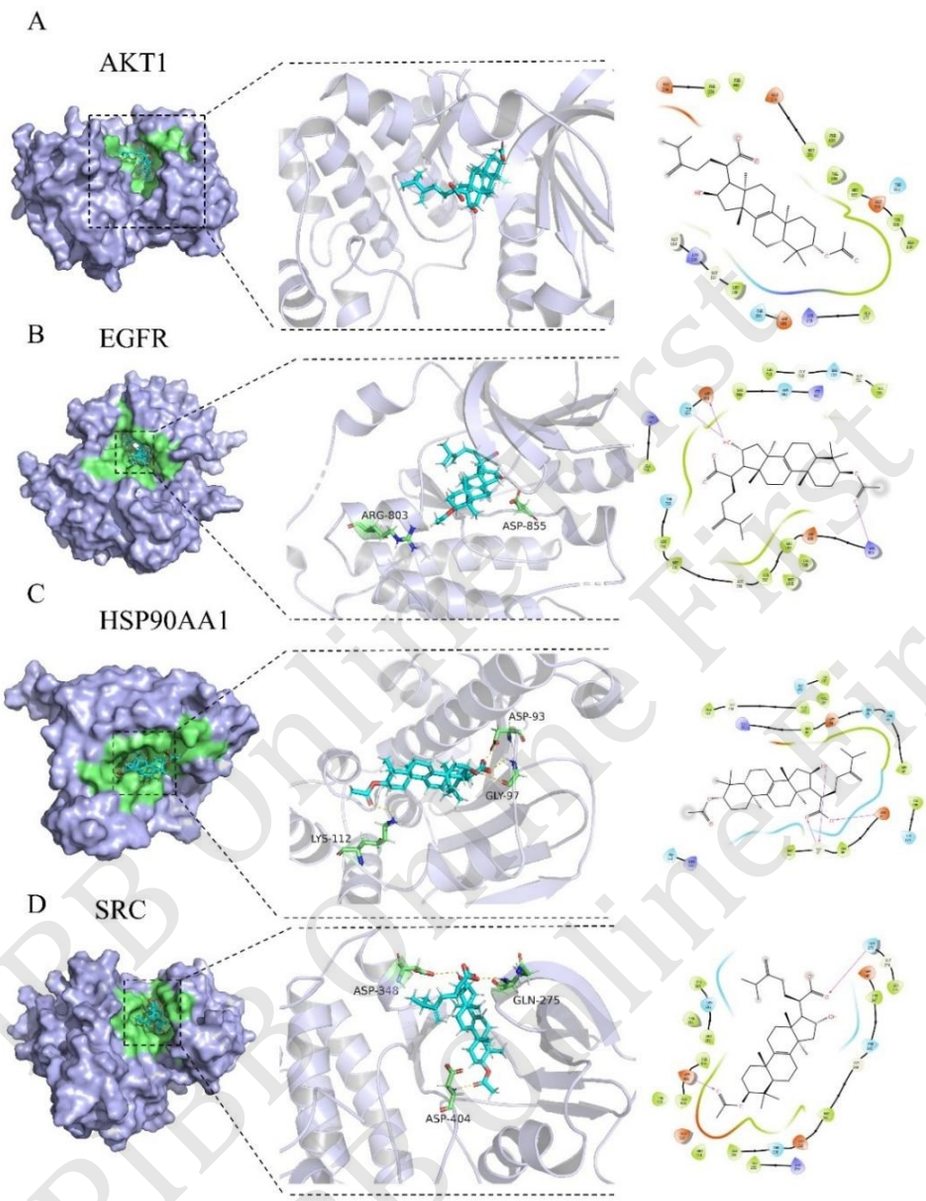

Fig. 2　Pictorial representation of the molecular interactions between cerevisterol and the top 4 targets

（a） Molecular docking model of PA with AKT1. （b） Molecular docking model of PA with SRC. （c） Molecular docking model of PA with EGFR. （d） Molecular docking model of PA with HSP90AA1.

Table 4　Molecular docking results

Ligand	PDBID	Receptor	Binding energy/（kcal · mol^{-1}）
PA	6CCY	AKT1	－8.2
PA	1XKK	EGFR	－7.5
PA	2BDF	SRC	－7.4
PA	2BYH	HSP90AA1	－7.3

conformations throughout the 100 ns molecular dynamics simulation. Similarly, the SASA analysis (Figure 4f) revealed minimal fluctuations in the solvent-accessible surface area, suggesting that ligand binding did not induce significant global conformational changes in the protein structures. The consistent SASA values imply that the surface exposure of residues remained stable, and that no significant unfolding or structural loosening occurred

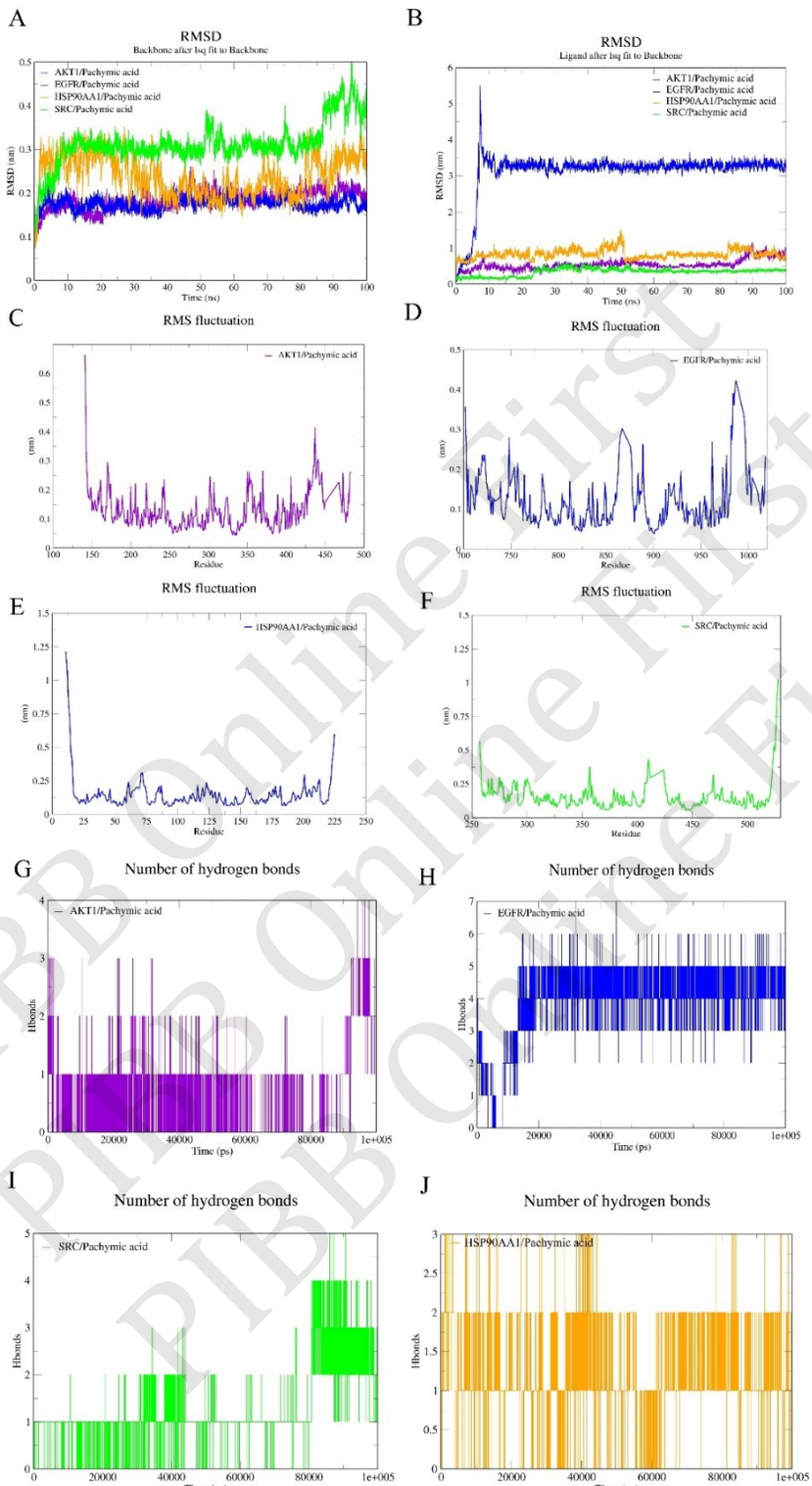

Fig. 3　Molecular dynamics simulation results of PA−target complex

（a） Root-mean-square deviation （RMSD） analysis of the backbone structures of AKT1， EGFR， HSP90AA1， and SRC complexes with PA over a 100 ns molecular dynamics （MD） simulation. （b） *RMSD* of PA as a ligand after alignment to the protein backbone in different complexes. （c－f） Root-mean-square fluctuation （*RMSF*） of protein residues in the AKT1/PA， EGFR/PA， HSP90AA1/PA， and SRC/PA complexes， respectively， indicating the flexibility of specific regions. The *y*-axis represents the RMSF values in nanometers （nm）， indicating the average atomic positional fluctuations of each residue over the course of the simulation. （g－j） Number of hydrogen bonds formed between PA and AKT1， EGFR， SRC， and HSP90AA1 during the MD simulation， demonstrating the stability of the ligand-protein interactions. The *y*-axis represents the number of hydrogen bonds formed between the ligand and the protein over the course of the simulation.

during ligand interactions. These findings suggest that the complexes retained their native-like structural integrity under dynamic equilibrium, which may contribute to reduced off-target interactions and lower toxicity risks, thereby supporting the potential of PA as a therapeutically favorable compound.

2.7.3 Hydrogen bond analysis

Hydrogen bonding plays a crucial role in ligand binding stability. The number of hydrogen bonds between PA and each target protein was monitored over time (Figure 3g – j). The PA-EGFR complex exhibited the greatest number of persistent hydrogen bonds, supporting the strong binding affinity observed in molecular docking. PA also formed stable hydrogen bonds with AKT1, HSP90AA1, and SRC, reinforcing the reliability of the docking results.

2.7.4 Gibbs free energy landscape

The Gibbs free energy landscape (Figure 4a – d) was constructed to analyze the conformational stability of the ligand-protein complexes. All the systems displayed a single deep energy basin, suggesting a stable binding mode with minimal conformational shifts. Notably, the PA-EGFR and PA-SRC complexes had the deepest free energy wells, which aligns with the strong binding affinities of these complexes observed in docking studies. The MD simulation results confirmed the stable binding of PA to all four core target proteins. The lower *RMSD*, stable Rg, and persistent hydrogen bonds indicate favorable interactions, whereas the Gibbs free energy analysis further supports the strong binding of PA to EGFR and SRC. These findings reinforce the hypothesis that PA exerts its therapeutic effects on NB through interactions with these core proteins.

2.8 MM/PBSA and per−residue decomposition analysis of four core proteins

In our study, the binding free energy and interaction energy components of the four compounds, AKT1, HSP90AA1, EGFR and SRC were analyzed using the MM-PBSA approach (Table 5, Figure S1a – d).

Binding energy decomposition analysis revealed that specific amino acid residues in AKT1, EGFR, SRC, and HSP90AA1 play crucial roles in PA binding. In the PA-AKT1 complex, residues such as ASP323, GLU328, and GLY178 exhibited notably strong binding affinities, contributing significantly to PA stabilization. Similarly, in the PA-EGFR complex, residues ASP855, GLU844, and GLU762 presented the strongest binding interactions, indicating key electrostatic and hydrogen bonding contributions. For the PA-HSP90AA1 complex, ASP93, GLU47, and GLY134 were the primary residues involved in stabilizing PA binding, further supporting the high binding affinity of PA to HSP90AA1 observed *via* RMSD analysis. Similarly, in the PA-SRC complex, ASP404, GLU310, and GLU329 play dominant roles in ligand binding, suggesting that these residues may be critical for PA-mediated modulation of SRC activity.

2.9 RT−qPCR validation of core gene expression

RT-qPCR analysis was conducted to assess the mRNA levels of these targets. Relative to the control group, PA treatment at concentrations of 10 μmol/L and 20 μmol/L for 24 h resulted in a significant decrease in the mRNA levels of AKT1, SRC, and EGFR. In contrast, the expression of HSP90AA1 was increased (Figure 5 a – d).

2.10 Validation of core protein expression by Western blot

To further validate the regulatory effects of PA on core targets at the protein level, Western blot analysis was performed on PA-treated N2a cells. Following 24 h of treatment with PA at concentrations of 10 μmol/L and 20 μmol/L, the protein expression levels of AKT1, SRC, and EGFR were significantly decreased (Figure 5e). Conversely, under the same treatment conditions, the protein expression of HSP90AA1 was markedly increased (Figure 5e).

3 Discussion

In this study network pharmacology was utilized to predict the potential protein targets of PA in NB, and these targets were validated through multidimensional approaches, including molecular docking, RT-qPCR, Western blot, and molecular dynamics simulations. Comprehensive analysis demonstrated that PA exerts anti-NB effects by targeting AKT1, EGFR, SRC, and HSP90AA1, with consistent modulation across transcriptional, translational, and conformational levels.

KEGG pathway analysis revealed that PA-targeted genes in NB are significantly enriched in the PI3K/AKT, MAPK, and Ras signaling pathways, supporting the hypothesis that PA exerts its antineuroblastoma effects *via* these pathways.

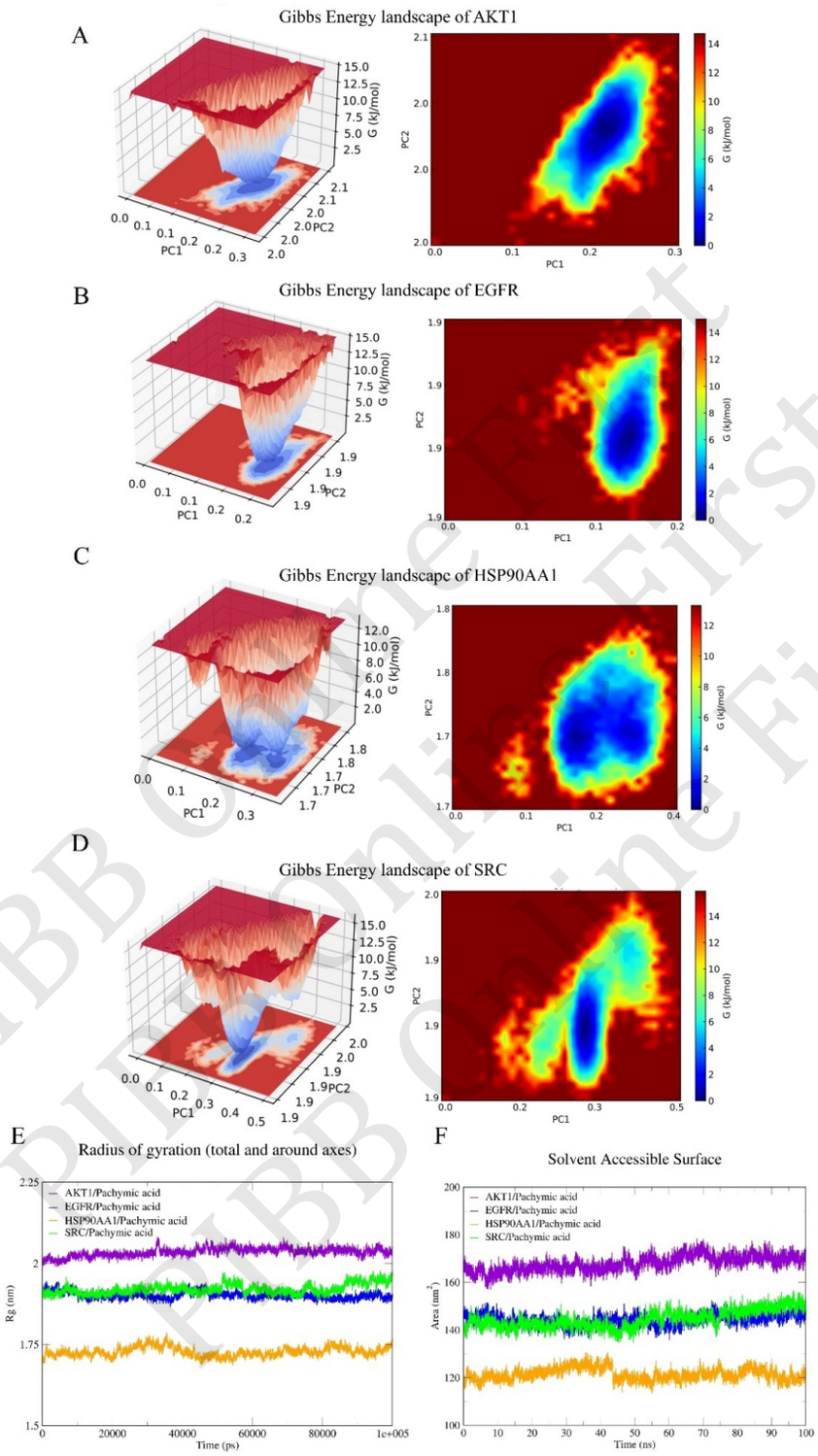

Fig. 4　Molecular dynamics simulation results of PA−target complex

（a－d） Gibbs free energy landscapes of AKT1， EGFR， HSP90AA1， and SRC in complex with PA. The three-dimensional energy landscapes （left） and corresponding two-dimensional projections （right） illustrate the conformational stability and energy minima of each protein-PA complex along principal component axes （PC1 and PC2）. Lower Gibbs energy regions （blue） indicate more stable conformational states. （e） Radius of gyration （Rg） analysis of AKT1， EGFR， HSP90AA1， and SRC complexes with PA over a 100 ns molecular dynamics （MD） simulation. Rg reflects the compactness and structural stability of the protein-ligand complexes. （f） Solvent-accessible surface area （SASA） of AKT1， EGFR， HSP90AA1， and SRC in complex with PA during the MD simulation， indicating changes in protein exposure to the solvent and potential binding stability.

Table 5　Binding free energy and detailed energy term contributions calculated by MM−PBSA method （kcal/mol）

	AKT1	HSP90AA1	EGFR	SRC
ΔG_{vdw}	－36.15	－19.93	3.04	－44.30
ΔG_{eel}	146.70	53.00	－151.91	－31.88
ΔG_{solv}	－123.40	－46.36	115.53	55.94
ΔG_{Total}	－12.86	－13.28	－33.34	－20.24

Notes: ΔG_{vdw}: van der Waals interactions, critical for shape complementarity and hydrophobic packing; ΔG_{eel}: electrostatic contributions, including hydrogen bonds and salt bridges; ΔG_{solv}: solvation effects, where polar/nonpolar terms balance desolvation penalties and hydrophobic gains; ΔG_{Total}: the sum of all terms, predicting overall binding affinity.

Western blot results indicated that PA treatment led to a concentration-dependent reduction in SRC, AKT1, and EGFR protein expression in N2a cells, which was consistent with the downregulation observed at the mRNA level *via* RT-qPCR. These results support the dual transcriptional-translational regulatory role of PA in modulating these targets. Integrating MD simulation data, this phenomenon can be mechanistically explained as follows: PA anchors to residues such as ASN391 and GLU310 through hydrogen bonding and hydrophobic interactions, stabilizing a closed SH2 domain conformation (*RMSD* <1.5 Å, 3－4 hydrogen bonds), thereby inhibiting its autophosphorylation at Tyr416 and reducing kinase activity. This inhibition likely triggers E3 ubiquitin ligase (*e.g.*, c-Cbl)-mediated proteasomal degradation, further downregulating transcription via negative feedback mechanisms (*e.g.*, miR-34a regulation)[27-28]. PA binding to AKT1 may prevent its membrane translocation and phosphorylation at Ser473, leading to the accumulation of inactive AKT1 in the cytoplasm and the suppression of its gene expression via the mTORC1-FOXO pathway[29].

Current studies have demonstrated aberrant expression and functional dysregulation of EGFR in various human malignant tissues and tumor cells[30]. EGFR primarily exerts its oncogenic effects through dimerization-induced stimulation of the Ras protein, leading to phosphorylation cascades that activate the PI3K/Akt signaling pathway. Importantly, EGFR activation recruits and phosphorylates SRC, thereby amplifying downstream PI3K/AKT and MAPK signaling pathways, which may serve as a critical driver for NB cell survival and metastasis[31]. The findings of the present study are consistent with the KEGG and GO analysis results obtained in our study. Furthermore, accumulating evidence has revealed that the EGFR/SRC/AKT1 axis plays pivotal roles in regulating cellular proliferation, survival, differentiation, and apoptosis processes in neuroblastoma cells[27]. The dynamic binding pattern of PA (*RMSD* ~3.0 Å) suggests ATP-competitive inhibition, which promotes EGFR ubiquitination and degradation while concurrently suppressing the EGFR/SRC/AKT1 signaling axis at both the transcriptional and translational levels[32].

Unlike those of SRC, AKT1, and EGFR, the protein and mRNA expression of HSP90AA1 were significantly decreased in a PA concentration-dependent manner. Previous studies have shown that under conditions of cellular stress, HSP90 stabilizes receptor proteins, preserving structural integrity and function. MD simulations revealed that PA interacts HSP90AA1 (backbone *RMSD* of ~3.5 Å, 1－3 hydrogen bonds), in a highly dynamic way, suggesting that PA does not form a rigid complex but may induce localized or dynamic conformational changes that interfere with HSP90 function rather than act as a direct strong binder. Such interference could activate heat shock factor 1 (HSF1)-mediated stress responses, triggering compensatory HSP90AA1 upregulation to maintain protein homeostasis[33]. However, the destabilization of client proteins by PA may counteract the prosurvival effects of HSP90 upregulation, ultimately leading to tumor cell death.

Although this study provides preliminary conclusions, further investigations are needed. Specifically, the biological significance of HSP90 compensation should be elucidated, including whether HSP90AA1 upregulation contributes to drug resistance and whether PA exhibits synergistic therapeutic effects with HSP90 inhibitors such as 17-AAG. Moreover, as the current findings are based on cellular experiments, *in vivo* studies are necessary to validate the reproducibility of target modulation and assess the therapeutic potential in animal models.

4　Conclusion

This study elucidates the multitarget anti-NB mechanism of PA through a combination of network pharmacology, molecular docking, RT-qPCR, and molecular dynamics simulations. PA preferentially stabilizes the inactive conformations of SRC and

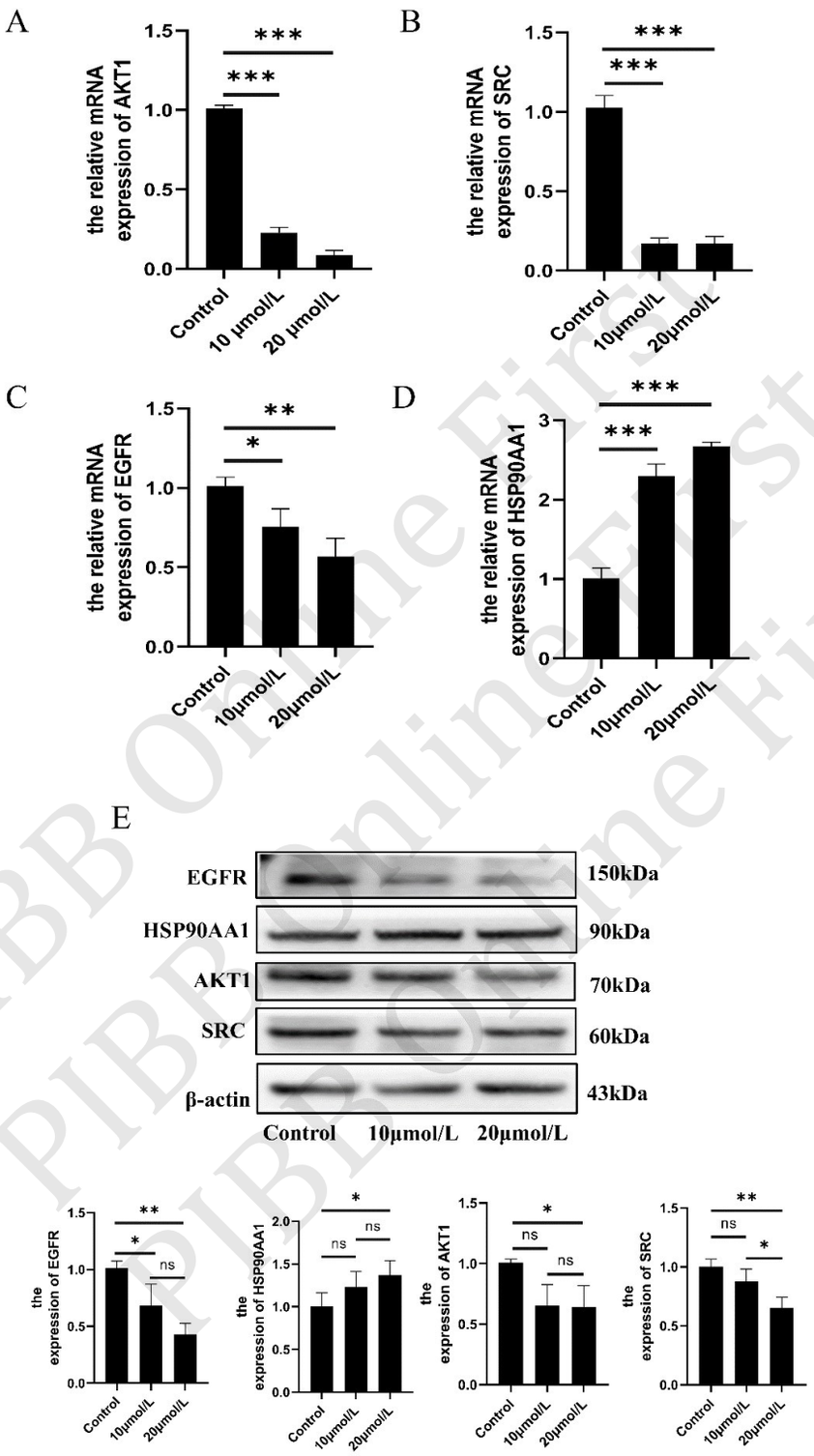

Fig. 5　Effects of PA on AKT1， SRC， EGFR， and HSP90AA1 expression at the mRNA and protein levels

Relative mRNA expression levels of AKT1， SRC， EGFR， and HSP90AA1 after treatment with different concentrations of PA. Changes in the mRNA expression of AKT1 （a）， SRC （b）， EGFR （c）， and HSP90AA1 （d） following treatment with different concentrations of PA. （e） Representative Western blot images and quantitative analysis showing dose-dependent downregulation of AKT1， SRC， and EGFR protein levels following 24 hours of treatment with PA （10 μmol/L and 20 μmol/L）. The data are presented as the mean±SD （n=3）. *P<0.05， **P<0.01， ***P<0.001 *vs*. control group.

AKT1 *via* high-affinity interactions, dynamically inhibits EGFR, and disrupts HSP90AA1-client protein interactions, collectively suppressing the PI3K/AKT, MAPK, and Ras signaling pathways. These findings not only advance our understanding of the polypharmacological effects of PA but also provide a structural foundation for rational drug design targeting NB.

Supplementary Available online (http://www.pibb.ac.cn, http://www.cnki.net): PIBB_20250154_Figure_S1.pdf

References

[1] Ward E, DeSantis C, Robbins A, *et al*. Childhood and adolescent cancer statistics, 2014. CA Cancer J Clin, 2014, **64**(2): 83-103

[2] Parsons K, Bernhardt B, Strickland B. Targeted immunotherapy for high-risk neuroblastoma—the role of monoclonal antibodies. Ann Pharmacother, 2013, **47**(2): 210-218

[3] Pinto N R, Applebaum M A, Volchenboum S L, *et al*. Advances in risk classification and treatment strategies for neuroblastoma. J Clin Oncol, 2015, **33**(27): 3008-3017

[4] Xiao Y, Hu Z, Liu H, *et al*. A review on antitumor effect of pachymic acid. Medicine (Baltimore), 2024, **103**(38): e39752

[5] Sun K X, Xia H W. Pachymic acid inhibits growth and induces cell cycle arrest and apoptosis in gastric cancer SGC-7901 cells. Oncol Lett, 2018, **16**(2): 2517-2524

[6] Chen Y, Lian P, Liu Y, *et al*. Pachymic acid inhibits tumorigenesis in gallbladder carcinoma cells. Int J Clin Exp Med, 2015, **8**(10): 17781-17788

[7] Wen H, Wu Z, Hu H, *et al*. The anti-tumor effect of pachymic acid on osteosarcoma cells by inducing PTEN and Caspase 3/7-dependent apoptosis. J Nat Med, 2018, **72**(1): 57-63

[8] Tan H L, Chan K G, Pusparajah P, *et al*. Anti-cancer properties of the naturally occurring aphrodisiacs: icariin and its derivatives. Front Pharmacol, 2016, **7**: 191

[9] Lai X, Wang X, Hu Y, *et al*. Editorial: network pharmacology and traditional medicine. Front Pharmacol, 2020, **11**: 1194

[10] Zhang P, Zhang D, Zhou W, *et al*. Network pharmacology: towards the artificial intelligence-based precision traditional Chinese medicine. Brief Bioinform, 2023, **25**(1): bbad518

[11] Li S. Framework and practice of network-based studies for Chinese herbal formula. J Chin Integr Med, 2007, **5**(5): 489-493

[12] Hopkins A L. Network pharmacology. Nat Biotechnol, 2007, **25**(10): 1110-1111

[13] Liu P Y, Hong K F, Liu Y D, *et al*. Total flavonoids of Astragalus protects glomerular filtration barrier in diabetic kidney disease. Chin Med, 2024, **19**(1): 27

[14] Wang Y, Yu Z, Zhang Z, *et al*. Integrating metabolomics with network pharmacology to reveal the mechanism of *Poria cocos* in hyperuricemia treatment. J Ethnopharmacol, 2025, **337**(Pt 3): 118977

[15] Zhang Y, Deng J, Tian H, *et al*. Design, synthesis, and bioevaluation of novel reversibly photoswitchable PI3K inhibitors based on phenylazopyridine derivatives toward light-controlled cancer treatment. J Med Chem, 2024, **67**(5): 3504-3519

[16] Huang D W, Sherman B T, Lempicki R A. Systematic and integrative analysis of large gene lists using DAVID bioinformatics resources. Nat Protoc, 2009, **4**(1): 44-57

[17] Ogata H, Goto S, Sato K, *et al*. KEGG Kyoto encyclopedia of genes and genomes. Nucleic Acids Res, 1999, **27**(1): 29-34

[18] Szklarczyk D, Gable A L, Lyon D, *et al*. STRING v11: protein-protein association networks with increased coverage, supporting functional discovery in genome-wide experimental datasets. Nucleic Acids Res, 2019, **47**(D1): D607-D613

[19] Kim S, Thiessen P A, Bolton E E, *et al*. PubChem substance and compound databases. Nucleic Acids Res, 2016, **44**(D1): D1202-D1213

[20] Ravindranath P A, Forli S, Goodsell D S, *et al*. AutoDockFR: advances in protein-ligand docking with explicitly specified binding site flexibility. PLoS Comput Biol, 2015, **11**(12): e1004586

[21] Huang J, MacKerell A D. CHARMM36 all-atom additive protein force field: Validation based on comparison to NMR data. J Comput Chem, 2013, **34**(25): 2135-2145

[22] Vanommeslaeghe K, Hatcher E, Acharya C, *et al*. CHARMM general force field: a force field for drug-like molecules compatible with the CHARMM all-atom additive biological force fields. J Comput Chem, 2010, **31**(4): 671-690

[23] Dolezal R, Soukup O, Malinak D, *et al*. Towards understanding the mechanism of action of antibacterial N-alkyl-3-hydroxypyridinium salts: biological activities, molecular modeling and QSAR studies. Eur J Med Chem, 2016, 121: 699-711

[24] Childers M C, Daggett V. Validating molecular dynamics simulations against experimental observables in light of underlying conformational ensembles. J Phys Chem B, 2018, **122**(26): 6673-6689

[25] Valdés-Tresanco M S, Valdés-Tresanco M E, Valiente P A, *et al*. gmx_MMPBSA: a new tool to perform end-state free energy calculations with GROMACS. J Chem Theory Comput, 2021, **17**(10): 6281-6291

[26] Yang H, Li G P, Liu Q, *et al*. Neuroprotective effects of Ginkgolide B in focal cerebral ischemia through selective activation of prostaglandin E2 receptor EP4 and the downstream transactivation of epidermal growth factor receptor. Phytother Res, 2021, **35**(5): 2727-2744

[27] Adams B D, Wali V B, Cheng C J, *et al*. miR-34a silences c-SRC to attenuate tumor growth in triple-negative breast cancer. Cancer Res, 2016, **76**(4): 927-939

[28] Yokouchi M, Kondo T, Sanjay A, *et al*. Src-catalyzed phosphorylation of c-Cbl leads to the interdependent ubiquitination of both proteins. J Biol Chem, 2001, **276**(37): 35185-35193

[29] Chen C C, Jeon S M, Bhaskar P T, *et al*. FoxOs inhibit mTORC1 and activate Akt by inducing the expression of Sestrin3 and Rictor. Dev Cell, 2010, **18**(4): 592-604

[30] Xu Z, Zhang M, Zhang X, *et al*. Dihydromyricetin protects against cisplatin-induced renal injury and mitochondria-mediated apoptosis *via* the EGFR/HSP27/STAT3 signaling pathway. Ren Fail, 2025, **47**(1): 2490202

[31] Karachaliou N, Cardona A F, Bracht J W P, *et al*. Integrin-linked kinase (ILK) and src homology 2 domain-containing phosphatase 2 (SHP2): novel targets in EGFR-mutation positive non-small cell lung cancer (NSCLC). EBioMedicine, 2019, 39: 207-214

[32] Singh S, Trevino J, Bora-Singhal N, *et al*. EGFR/Src/Akt signaling modulates Sox2 expression and self-renewal of stem-like side-population cells in non-small cell lung cancer. Mol Cancer, 2012, **11**: 73

[33] Zuehlke A D, Beebe K, Neckers L, *et al*. Regulation and function of the human HSP90AA1 gene. Gene, 2015, **570**(1): 8-16

网络药理学结合实验验证揭示茯苓酸治疗神经母细胞瘤的作用机制*

刘　航[1,2)]　祝雨欣[1)]　郭思霖[1)]　潘信运[1)]　谢远杰[2,3)]　廖思聪[4)]　戴鑫汶[5)]
申　平[2,3)**]　肖玉波[1,4)**]

([1)] 湖南医药学院检验医学院，湖南省中药合成生物学重点实验室，怀化 418000；
[2)] 桂林医科大学广西糖尿病系统医学重点实验室，桂林 541199；
[3)] 邵东市人民医院，邵东市人民医院-明舜制药转化医学联合实验室，邵东 422800；
[4)] 桂林医科大学附属医院，广西肝损伤与修复分子医学重点实验室，桂林 541001；
[5)] 湖南补天药业有限公司专家工作站，长沙 410000）

摘要　目的　本研究旨在通过网络药理学、分子动力学与实验验证等方法，探究茯苓酸（pachymic acid，PA）在治疗神经母细胞瘤（neuroblastoma，NB）中的潜在分子靶点及其作用机制。**方法**　本研究首先基于网络药理学方法筛选PA可能作用于NB的靶点，随后结合分子对接、分子动力学（MD）模拟、MM/PBSA自由能计算及RT-qPCR、Western blot实验进行多维度验证。**结果**　CCK-8实验显示，PA对NB细胞具有浓度依赖性的抑制作用。KEGG通路富集分析提示，PA的抗NB作用可能通过调控PI3K-Akt、MAPK及Ras等信号通路实现。分子对接及分子动力学模拟结果表明，PA可与AKT1、EGFR、SRC及HSP90AA1等核心靶蛋白稳定结合。RT-qPCR与Western blot分析进一步证实，PA处理可显著下调AKT1、EGFR及SRC的mRNA和蛋白质表达水平，同时上调HSP90AA1的表达水平。**结论**　茯苓酸可能通过抑制AKT1、EGFR和SRC的表达，调控PI3K/AKT信号通路，从而发挥其抗神经母细胞瘤作用。研究结果为PA在NB治疗中的潜在应用提供了重要的实验依据。

关键词　茯苓酸，网络药理学，分子动力学
中图分类号　R285　　**DOI**：10.16476/j.pibb.2025.0154　　**CSTR**：32369.14.pibb.20250154

* 湖南省自然科学基金（2023JJ50440），广西自然科学基金（2025GXNSFHA069221），湖南省教育厅科学研究基金（22A0707），国家级大学生创新创业训练计划（S202212214001），广西卫健委糖脂代谢相关疾病基础研究重点实验室（GKLBRSMR-K202403）和邵东市人民医院横向合作科研项目（2023SDHX02）资助。
** 通讯联系人。
申平　Tel：0739-2721153，E-mail：shenpsd@126.com
肖玉波　Tel：0745-2381486，E-mail：yuboxiaohn@126.com
收稿日期：2025-04-09，接受日期：2025-06-13